energies

MDPI

Article

Enhanced Thermoelectric Characteristics of Ag_2Se Nanoparticle Thin Films by Embedding Silicon Nanowires

Seunggen Yang, Kyoungah Cho * and Sangsig Kim *

Department of Electrical Engineering, Korea University, Seoul 02841, Korea; cacamura@korea.ac.kr
* Correspondence: chochem@korea.ac.kr (K.C.); sangsig@korea.ac.kr (S.K.);
Tel.: +82-2-3290-3909 (K.C. & S.K.); Fax: +82-2-921-0544 (K.C. & S.K.)

Received: 4 May 2020; Accepted: 10 June 2020; Published: 13 June 2020

Abstract: A solution-processable Ag_2Se nanoparticle thin film (NPTF) is a prospective thermoelectric material for plastic-based thermoelectric generators, but its low electrical conductivity hinders the fabrication of high performance plastic-based thermoelectric generators. In this study, we design Ag_2Se NPTFs embedded with silicon nanowires (SiNWs) to improve their thermoelectric characteristics. The Seebeck coefficients are −233 and −240 μV/K, respectively, for a Ag_2Se NPTF alone and a Ag_2Se NPTF embedded with SiNWs. For the Ag_2Se NPTF embedded with SiNWs, the electrical conductivity is improved from 0.15 to 18.5 S/m with the embedment of SiNWs. The thermal conductivities are determined by a lateral thermal conductivity measurement for nanomaterials and the thermal conductivities are 0.62 and 0.84 W/(m·K) for a Ag_2Se NPTF alone and a Ag_2Se NPTF embedded with SiNWs, respectively. Due to the significant increase in the electrical conductivity and the insignificant increase in its thermal conductivity, the output power of the Ag_2Se NPTF embedded with SiNWs is 120 times greater than that of the Ag_2Se NPTF alone. Our results demonstrate that the Ag_2Se NPTF embedded with SiNWs is a prospective thermoelectric material for high performance plastic-based thermoelectric generators.

Keywords: thermoelectric; silver selenide nanoparticles; silicon nanowires; thin film

1. Introduction

Thermoelectric generators for energy conversion from ambient heat to electricity have been widely developed in the area of renewable energy [1,2]. High electrical conductivity and low thermal conductivity are essential in achieving high thermoelectric efficiency, but the independent control of each other is fraught with challenges. Nanosized semiconductor materials are suitable for thermoelectric materials because of their independent control of electrical and thermal conductivities [1–3]. As one way to make nanosized semiconductor materials, solution processes have been regarded as an attractive approach for the fabrication of next-generation flexible electronics since they have the potential advantages of low synthetic temperatures, large area processes, low cost and compatibilities with plastic substrates [4–6]. Moreover, with a rapid increase in the necessity of flexible electronics and miniature sensors, thermoelectric devices fabricated on flexible and bendable substrates have been considered as one component part in power supply systems for flexible electronics and miniature sensors [7,8]. On the other hand, among nanosized semiconductor materials, solution-processable semiconductor nanoparticles (NPs), such as mercury chalcogenide [4] and silver chalcogenide [5] NPs, have emerged as thermoelectric materials for plastic-based thermoelectric generators [6] because they are processed at sufficiently low temperatures compared to the thermal degradation temperature of plastic substrates. In particular, silver selenide (Ag_2Se) NPs have been studied as a promising thermoelectric

nanomaterial for high efficiency thermoelectric devices, due to their high mobility and low thermal conductivity [9,10]. Hence, in this study, we chose Ag_2Se NPs to represent solution-processable semiconductor NPs.

To fabricate high-performance plastic-based thermoelectric generators, increasing the electrical conductivity of thin films composed of the solution-processable semiconductor NPs is essential. The increase in electrical conductivity inevitably leads to an increase in thermal conductivity. To achieve high thermoelectric conversion efficiency, it is necessary to enhance electrical conductivity while simultaneously lowering the thermal conductivity of thermoelectric materials as required. There have been various approaches, such as doping [3], annealing [11], optimizing structure [12], and developing new and advanced thermoelectric nanomaterials [13] to improve the thermoelectric characteristics. Nevertheless, a hetero-dimensional combination of nanomaterials has not been investigated as a means of improving the thermoelectric properties of thin films composed of the solution-processable semiconductor NPs that are suitable for plastic-based thermoelectric generators. Hence, for the first time, we attempt to combine one-dimensional nanowires and the two-dimensional nanoparticle thin films (NPTFs) as a way to develop thermoelectric materials for high-performance plastic-based thermoelectric generators.

In this study, we propose a NPTF embedded with nanowires (NW). We chose NWs because, among nanosized semiconductor materials, NWs are favorable for electrical conduction [14–16]. More specifically, we embedded silicon NWs (SiNWs) in an Ag_2Se NPTF to increase its electrical conductivity considerably as compared to the thermal conductivity [16,17]. In this study, we employed SiNWs fabricated from a Si wafer by the top-down process, in which the physical properties of SiNWs are similar with those of the mother Si wafer. The etched SiNWs with rough edges tend to reduce heat transfer of phonons, while electrons are hardly affected by the roughness of their surfaces [16]. Due to their rough edges, the SiNWs have received great interest for dramatically improving the thermoelectric properties of Si [16,17]. Compared with other semiconductor NWs, such as chalcogenides [18–20], our SiNWs are well-ordered and transferred on the plastic substrate, which is a key point for the fabrication of the Ag_2Se NPTF embedded with SiNWs. In addition, SiNWs are suitable for plastic-based thermoelectric devices since they are able to be transferred on plastic substrates without deterioration in electrical characteristics of Si. To measure the thermal conductivity of the Ag_2Se NPTF embedded with SiNWs, we adopted a lateral thermal conductivity measurement for nanomaterials [21–23]. In this study, we evaluated the suitability of the Ag_2Se NPTF embedded with SiNWs as a thermoelectric material by comparing it with the Ag_2Se NPTF alone.

2. Materials and Methods

Figure 1 shows the Ag_2Se NPTF alone and the Ag_2Se NPTF embedded with SiNWs on a polyethersulfone (PES, CAS No. 25667-42-9) plastic substrate. The *n*-SiNWs were prepared through CMOS-compatible top-down approaches, and the Ag_2Se NPs were synthesized by the colloidal method, as depicted in previous research [22,24]. The *n*-SiNWs with an arsenic doping concentration of 10^{21} cm^{-3} were prepared by the top-down process using photolithography, crystallographic wet etching, ion implantation doping, and size reduction thermal oxidation as shown in Figure 2a–c. Then, the *n*-SiNWs with a 40 nm thickness were transferred onto the plastic substrate via a direct transfer process as shown in Figure 2d–i. Figure 2j is the SEM image of SiNWs transferred onto a PES substrate. Ag_2Se NPs used as a thermoelectric nanomaterial in this study were synthesized in an aqueous solution in the following steps [24]: 1 mL of 1-thioglycerol (CAS No. 96-27-5) and 0.3 g of $AgNO_3$ (CAS No. 7761-88-8) were dissolved in 250 mL of distilled water via stirring. The pH of the mixed solution was adjusted to 11.4 with 1 M NaOH solution (CAS No. 1310-73-2). Ag_2Se NPs were then obtained by the reaction of the Ag_2Se NPs solution and H_2Se gas. Herein H_2Se gas was produced by the reaction of 0.2 g of Al_2Se_3 (CAS No. 1302-82-5) and 50 mL of 4 M HCl solution (CAS No. 7647-01-0). Ag_2Se NP powders were subsequently made using a centrifugation process and were then re-dispersed in deionized water. Re-dispersed Ag_2Se NPs solution was made by dispersing 1 mg

of Ag_2Se NPs produced by centrifugation in 10 µL of distilled water. A thermoelectric platform was constructed using two electrodes (E1 and E2), a meander line patterned heater made of Al, and a thermoelectric channel on a plastic substrate. Herein, the heater and two electrodes were fabricated through photolithography and thermal evaporation processes for 5 min at a working pressure of 6 mTorr, and then the Ag_2Se NPTF was coated through photolithography and a spin-coating process at 4000 rpm for 35 s between the two electrodes. We made the surface of the patterned substrate hydrophilic using O_2 plasma before spin-coating of the Ag_2Se NPTF on a plastic substrate. The diameter of the Ag_2Se NP and the thickness of the Ag_2Se NPTF were measured to be 5 nm and 30 nm from images taken by a transmission electron microscope (TECNAI F20), respectively, as shown in Figure 3. In this study, we used two thermoelectric channel materials: Ag_2Se NPTF alone and Ag_2Se NPTF embedded with SiNWs. For both thermoelectric channel materials, only the Ag_2Se NPTFs were in contact with E1 and E2; the SiNWs were not in contact with E1 and E2. The distance between E1 and E2 was 200 µm and the length of the SiNWs was 100 µm. The thermoelectric characteristics of the fabricated thermoelectric devices were investigated through a Keithley 4200 parameter analyzer and infrared (IR) images were captured using a FLIR A645SC IR camera with sensitivity of 30 mK and an uncertainty of 2%. The thermal conductivities of the Ag_2Se NPTF alone and the Ag_2Se NPTF embedded with SiNWs were measured using the lateral thermal conductivity measurement, as described in previous studies [21,22]. In this study, all measurements of thermoelectric devices were carried out at room temperature in a vacuum condition of 10^{-6} Torr.

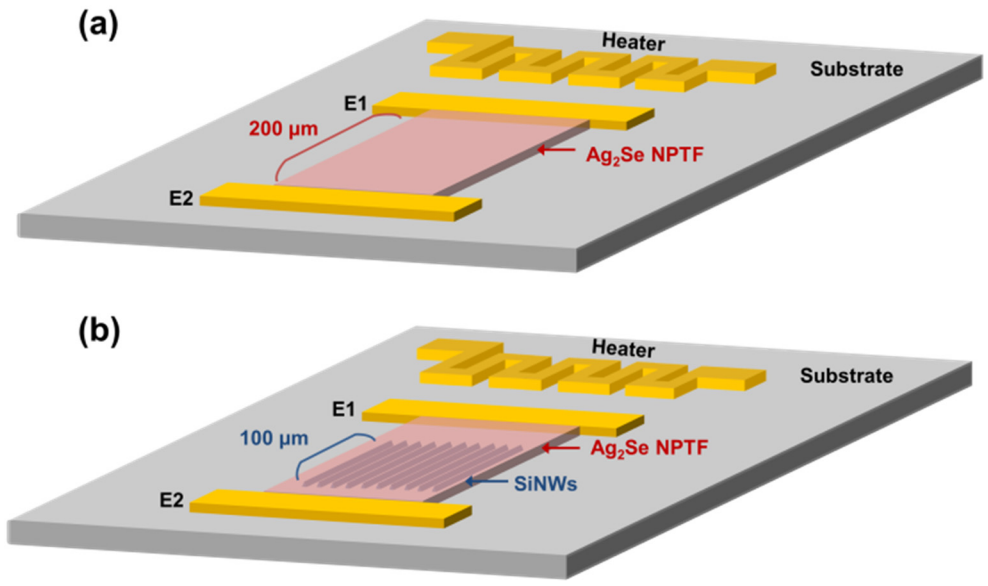

Figure 1. Schematic of a thermoelectric platform comprising a meander line patterned heater, two electrodes (E1, E2), and thermoelectric channels of (**a**) the Ag_2Se nanoparticle thin film (NPTF) alone and (**b**) the Ag_2Se NPTF embedded with silicon nanowires (SiNWs).

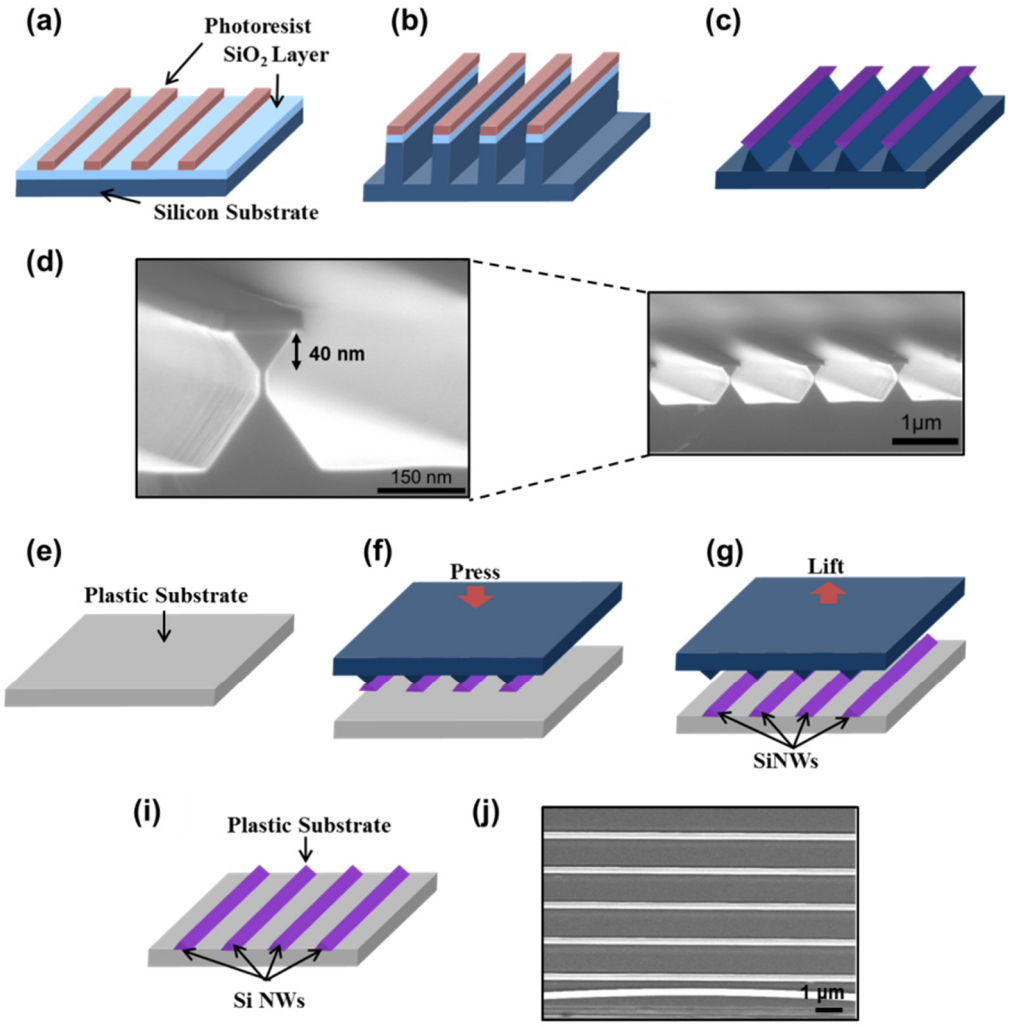

Figure 2. Fabrication process of the SiNWs. (**a**) Si active lines on an oxide stack. (**b**) Si trench etching. (**c**) Crystallographic wet etching. (**d**) SEM images of fabricated SiNWs. (**e**–**i**) transfer process of SiNWs on plastic substrate. (**j**) SEM image of transferred SiNWs.

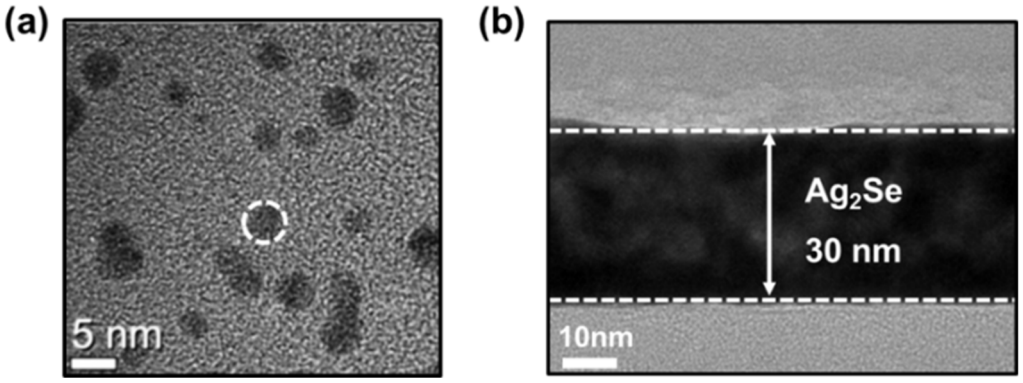

Figure 3. TEM images of the Ag_2Se NPs (**a**) and cross-sectional image (**b**) of the Ag_2Se NP thin film.

3. Results and Discussion

Figure 4 displays optical images of the Ag_2Se NPTF alone (a) and the Ag_2Se NPTF embedded with SiNWs (b), and shows that the SiNWs were well covered with the Ag_2Se NPTF but that they maintained a distance from the electrodes E1 and E2. In this study, the temperature difference (ΔT) caused by joule heating of the heater is defined as the difference in temperature between the hot electrode E1

and cold electrode E2, as the temperatures of those parts of the NPTF in contact with the electrodes were the same as those of the corresponding electrodes. By contrast, thermal energy caused by the heater was propagated through thermal conduction of the thermoelectric channel ($Q_{thermoelectric\ channel}$) and thermal radiation ($Q_{radiation}$) and the substrate ($Q_{substrate}$). In the case without any thermoelectric channel, the ΔT was caused by $Q_{radiation}$ and $Q_{substrate}$, whereas in the case with a thermoelectric channel, the ΔT is caused by $Q_{radiation}$, $Q_{substrate}$ and $Q_{thermoelectric\ channel}$. Thus, the $Q_{thermoelectric\ channel}$ was determined by the difference between the temperatures of E2 for the cases with and without the thermoelectric channel.

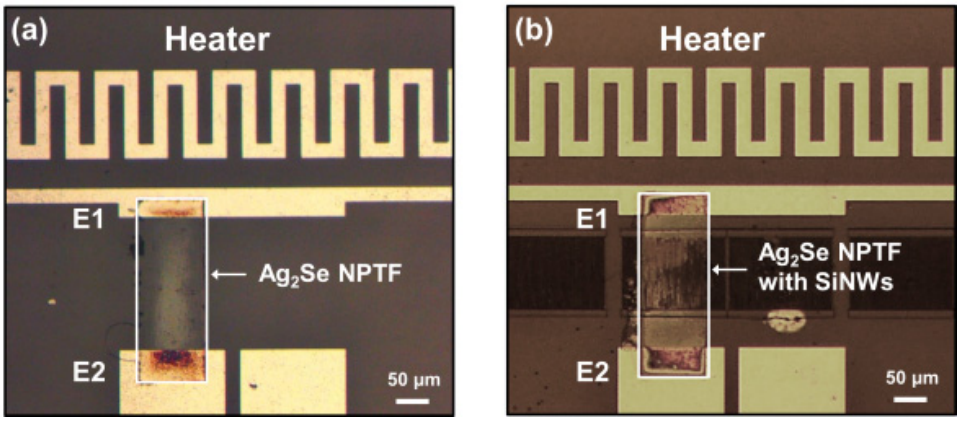

Figure 4. Optical image of a thermoelectric platform comprising a meander line patterned heater, two electrodes (E1, E2), and thermoelectric channels of (**a**) the Ag_2Se NPTF alone and (**b**) the Ag_2Se NPTF embedded with SiNWs.

To measure the thermal conductivities of the Ag_2Se NPTF alone and the Ag_2Se NPTF embedded with SiNWs, the temperatures of E2 were measured as a function of heater power, as depicted in Figure 5a,b, respectively. Herein, the heater power has the proportional relationship with the temperatures of E1 because a large amount of heat is transferred to E1 as the heater power increases. As previously mentioned, the difference between the temperatures of E2 for the cases with and without the thermoelectric channel was attributed to the $Q_{thermoelectric\ channel}$. The temperature difference was induced by the $Q_{thermoelectric\ channel}$ for the Ag_2Se NPTF alone and the Ag_2Se NPTF embedded with SiNWs as a function of heater power, as depicted in Figure 5c, indicating that thermal energy was more quickly transferred in the Ag_2Se NPTF embedded with SiNWs than in the Ag_2Se NPTF alone. The thermal conductivity of the thermoelectric channel was calculated based on the heat conduction law known as Fourier's law. The lateral heat conduction of thermoelectric channel was calculated by the equation as follows [25]:

$$Q = \kappa A dT/dx \quad (1)$$

where Q is the heat conduction of the thermoelectric channel, κ is the thermal conductivity, A is the cross-sectional area, and dT/dx is the temperature gradient of the lateral direction. The value of Q can be calculated from the value of heater power corresponding to the temperature of E1 because the heater and E1 were composed of the same material in this study. The heat flux (q″) of the thermoelectric channel is Q per unit area perpendicular to the direction of heat flow. Since the hot and cold sides of the thermoelectric channel were thermally balanced with E1 and E2, respectively, the lateral heat flux of the thermoelectric channel was given by the equation as follows [26]:

$$q'' = \kappa \Delta T/\Delta x \quad (2)$$

where ΔT is the temperature difference and Δx is the distance between E1 and E2. Figure 5d shows q″ as a function of $\Delta T/\Delta x$. The slope in the graph indicates the thermal conductivity. This means that the thermal conductivities of the Ag_2Se NPTF alone and the Ag_2Se NPTF embedded with SiNWs were

calculated to be 0.62 and 0.84 W/(m·K), respectively. The thermal conductivity of the Ag_2Se NPTF embedded with SiNWs was slightly higher than that of the Ag_2Se NPTF alone, which is consistent with the result shown in Figure 5c. Compared to the thermal conductivity of SiNWs (about 40 W/(m·K)) [15], the remarkably low thermal conductivity of the Ag_2Se NPTF embedded with SiNWs results from phonon scattering at the grain boundaries of the Ag_2Se NPTF covering the SiNWs. On the other hand, the lateral thermal conductivity measurement method used in this study is the most appropriate to examine the thermal conductivity of hetero-dimensional combined nanomaterials that are impossible to measure the thermal conductivity using conventional thermal conductivity measurement methods such as the laser flash method or the three omega method [27–29]. Generally, the conventional thermal conductivity measurement methods require the smooth surface and the thickness greater than one millimeter for a sample, which is hard to make with nanomaterials.

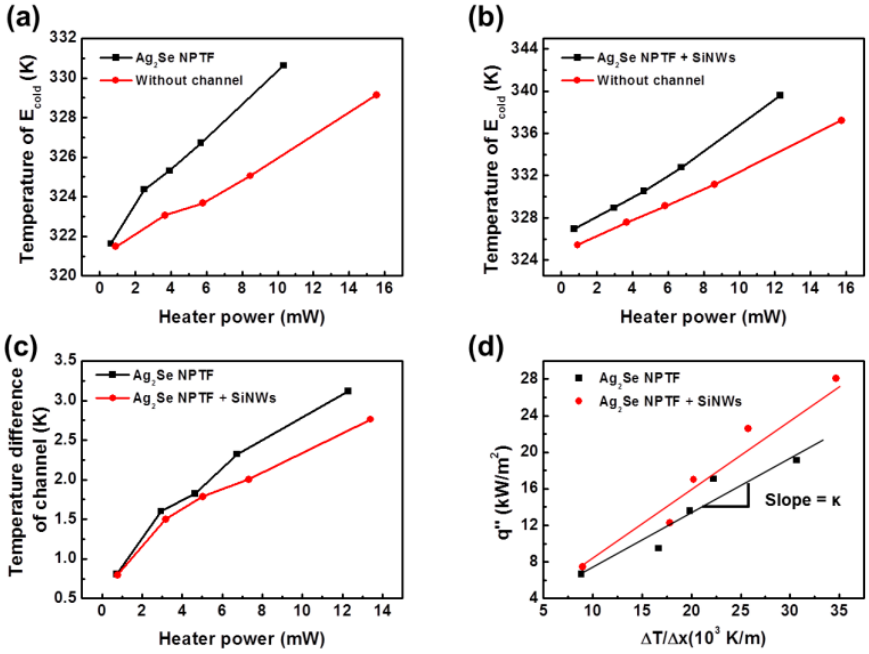

Figure 5. Temperature of E2 for (**a**) the Ag_2Se NPTF alone and (**b**) the Ag_2Se NPTF embedded with SiNWs. (**c**) Temperature difference of the channel as a function of heater power. (**d**) q″ versus ΔT/Δx.

Figure 6a represents the current–voltage characteristics of the Ag_2Se NPTF alone and the Ag_2Se NPTF embedded with SiNWs. The magnitude of current in the Ag_2Se NPTF embedded with SiNWs increased by more than 100 times due to the SiNWs being embedded into the Ag_2Se NPTF. The electrical conductivities of the Ag_2Se NPTF alone and the Ag_2Se NPTF embedded with SiNWs were calculated at 0.15 and 18.5 S/m, respectively. Bearing in mind that the thermal conductivity of the Ag_2Se NPTF insignificantly increases from 0.62 to 0.84 W/(m·K) by the embedment of SiNWs, it is clear that the embedment of SiNWs into the Ag_2Se NPTF is a useful way to increase the electrical conductivity of the Ag_2Se NPTF restraining the increase in its thermal conductivity. Compared to other studies [7,8] in which the thermal conductivity of a thermoelectric material increases as its electrical conductivity increases at the same rate, our result shows the increase in the electrical conductivity that is relatively independent from the thermal conductivity. The enhanced electrical conductivity in the Ag_2Se NPTF embedded with SiNWs implies that inserting SiNWs to solution-processable NPTFs is an effective way to increase electrical conductivity of NPTFs for plastic-based thermoelectric generators. Figure 6b represents the Seebeck voltages as a function of ΔT for the Ag_2Se NPTF alone and the Ag_2Se NPTF embedded with SiNWs, indicating their *n*-type behaviors. The Seebeck coefficients obtained from the slope in Figure 6b were −233 and −240 μV/K for the Ag_2Se NPTF alone and the Ag_2Se NPTF embedded with SiNWs, respectively. The maximum Seebeck voltages are −2.7 and −2.4 mV at ΔT of

11.7 and 9.1 K, respectively, for the Ag_2Se NPTF alone and the Ag_2Se NPTF embedded with SiNWs. It is worthy of note that the Seebeck voltages are generated from the temperature difference of about 10 K at room temperature. On the other hand, considering the inverse relationship between the Seebeck coefficient and electrical conductivity, the Ag_2Se NPTF embedded with SiNWs proposed in this study is a promising high-performance thermoelectric material because it exhibits a uniquely higher Seebeck coefficient and a higher electrical conductivity than those of the Ag_2Se NPTF alone. The thermoelectric power factors ($PF = S^2\sigma$; S is the Seebeck coefficient and σ is the electrical conductivity) were determined to be 8.1×10^{-3} and 1.1 $\mu W/(m \cdot K^2)$ for the Ag_2Se NPTF alone and the Ag_2Se NPTF embedded with SiNWs, respectively. The figure of merit (ZT) was calculated as 3.9×10^{-5} and 3.8×10^{-3} for the Ag_2Se NPTF alone and the Ag_2Se NPTF embedded with SiNWs, respectively. The significant increase in PF and ZT of the Ag_2Se NPTF embedded with SiNWs was attributed to the greatly increased electrical conductivity as compared with the thermal conductivity. In terms of plastic-based thermoelectric generators, the considerable increase in the PF and ZT for a solution-processable NPTF is fundamental to achieving high performance thermoelectric generators that convert a bit of heat to electricity at room temperature. Figure 6c exhibits the output power (P) as a function of ΔT for the Ag_2Se NPTF alone and the Ag_2Se NPTF embedded with SiNWs. The P was calculated as per [30]:

$$P = \frac{V_S^2}{4R} \tag{3}$$

where R is the resistance of the thermoelectric channel and V_S is the Seebeck voltage, indicating an inverse relationship between the resistance and output power of the thermoelectric channel. The output powers generated from the Ag_2Se NPTF embedded with SiNWs and the Ag_2Se NPTF alone were 2.8 and 2.3×10^{-2} nW/cm^2, respectively, at a ΔT of 9.1 K. Due to the dramatic improvement in the electrical conductivity through embedment of SiNWs, the maximum output power of the Ag_2Se NPTF embedded with SiNWs was 120 times greater than that of the Ag_2Se NPTF alone. To enhance the maximum output power, lowering the resistance of the thermoelectric channel is critical. Even though sintering is a conventional means of lowering the resistance of the thermoelectric channel, it is unsuitable for plastic-based thermoelectric devices because the sintering temperature is sufficiently high to degrade the plastic. As such, the Ag_2Se NPTF embedded with SiNWs is effective at lowering the resistance of the thermoelectric channel on a plastic substrate. Furthermore, our result demonstrates that a small amount of thermal energy coming from the surrounding environment can be effectively converted to electrical energy by the Ag_2Se NPTF embedded with SiNWs, which can be used in practical applications, such as portable, flexible electronics and miniature sensors.

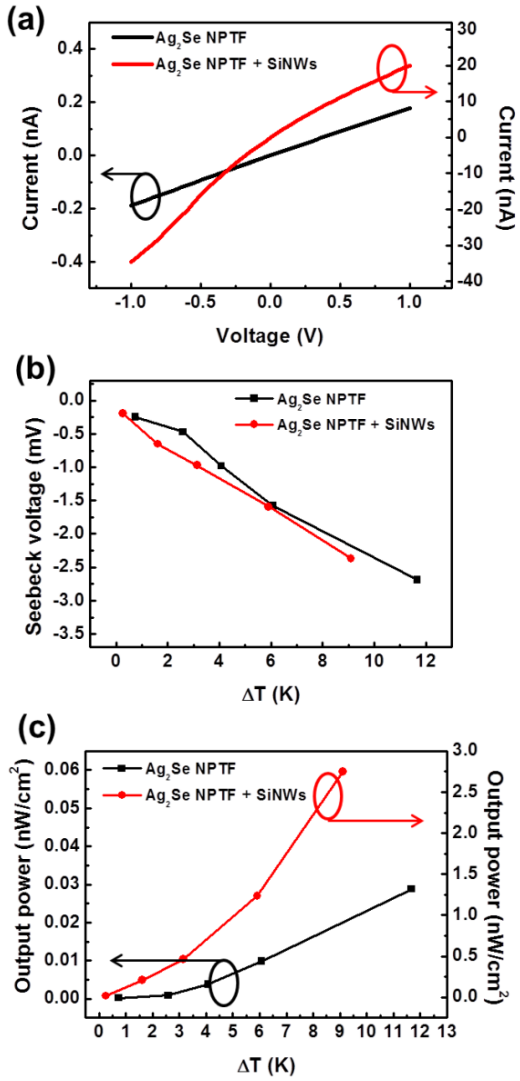

Figure 6. (**a**) Current–voltage characteristics, (**b**) Seebeck voltage, and (**c**) output power as a function of temperature difference for the Ag_2Se NPTF alone and the Ag_2Se NPTF embedded with SiNWs.

4. Conclusions

In this study, we embed SiNWs in a solution-processed Ag_2Se NPTF to increase the electrical conductivity of the solution-processable NPTFs for high-performance plastic-based thermoelectric generators. The Ag_2Se NPTF alone and the Ag_2Se NPTF embedded with SiNWs exhibited *n*-type behavior. Because of the SiNWs, the Ag_2Se NPTF embedded with SiNWs had an electrical conductivity that was 120 times greater than that of the Ag_2Se NPTF alone. The electrical conductivities of the Ag_2Se NPTF alone and the Ag_2Se NPTF embedded with SiNWs were 0.15 and 18.5 S/m, respectively. For the Ag_2Se NPTF alone and the Ag_2Se NPTF embedded with SiNWs, the Seebeck coefficients were −233 and −240 μV/K, respectively. Compared to the increase in the electrical conductivity, thermal conductivity was insignificantly increased from 0.62 to 0.84 W/(m·K) by embedding SiNWs in the Ag_2Se NPTF. Due to the dramatic improvement in electrical conductivity through embedment of SiNWs, the Ag_2Se NPTF embedded with SiNWs generated the maximum output power that was 120 times greater than the Ag_2Se NPTF alone. Our results demonstrate that the Ag_2Se NPTF embedded with SiNWs is a prospective thermoelectric material for converting low-grade thermal energy into electrical energy in actual applications such as portable plastic electronics.

Author Contributions: All authors have cooperated in the preparation of this work. Conceptualization, S.Y., K.C. and S.K.; methodology, S.Y., K.C. and S.K.; validation, S.Y. and K.C.; formal analysis, K.C. and S.K.; investigation, S.Y. and K.C.; resources, K.C. and S.K.; data curation, S.Y., K.C. and S.K.; writing—original draft preparation, S.Y., K.C. and S.K.; writing—review and editing, S.Y., K.C. and S.K.; visualization, K.C. and S.K.; project administration, K.C. and S.K.; All authors have read and agreed to the published version of the manuscript.

Funding: This research was funded by [the Technology Development Program to Solve Climate Changes] grant number [NRF-2017M1A2A2087323]. And [the Brain Korea 21 Plus Project] in 2020 through the National Research Foundation of Korea (NRF) funded by the Ministry of Science, ICT & Future Planning, and a Korea University Grant.

Conflicts of Interest: The authors declare no conflict of interest.

References

1. Snyder, G.J.; Toberer, E.S. Complex thermoelectric materials. *Nat. Mater.* **2008**, *7*, 105–114. [CrossRef] [PubMed]
2. Zhang, Q.; Ai, X.; Wang, L.; Chang, Y.; Luo, W.; Jiang, W.; Chen, L. Improved thermoelectric performance of silver nanoparticles-dispersed Bi_2Te_3 composites deriving from hierarchical two-phased heterostructure. *Adv. Funct. Mater.* **2015**, *25*, 966–976. [CrossRef]
3. Alam, H.; Ramakrishna, S. A review on the enhancement of figure of merit from bulk to nano-thermoelectric materials. *Nano Energy* **2013**, *2*, 190–212. [CrossRef]
4. Yun, Y.; Cho, K.; Park, Y.; Yang, S.; Choi, J.; Kim, S. Thermoelectric characteristics of nanocomposites made of HgSe and Ag nanoparticles for flexible thermoelectric devices. *Nano Res.* **2017**, *10*, 683–689. [CrossRef]
5. Choi, J.; Cho, K.; Yun, J.; Park, Y.; Yang, S.; Kim, S. Large voltage generation of flexible thermoelectric nanocrystal thin films by finger contact. *Adv. Energy Mater.* **2017**, *7*, 1700972. [CrossRef]
6. Chen, Y.N.; Zhao, Y.; Liang, Z.Q. Solution processed organic thermoelectrics: Towards flexible thermoelectric modules. *Energy Environ. Sci.* **2015**, *8*, 401–422. [CrossRef]
7. Suarez, F.; Nozariasbmarz, A.; Vashaee, D.; Ozturk, M.C. Designing thermoelectric generators for self-powered wearable electronics. *Energy Environ. Sci.* **2016**, *9*, 2099–2113. [CrossRef]
8. Bahk, J.H.; Fang, H.Y.; Yazawa, K.; Shakouri, A. Flexible thermoelectric materials and device optimization for wearable energy harvesting. *J. Mater. Chem. C* **2015**, *3*, 10362. [CrossRef]
9. Wang, H.; Chu, W.; Wang, D.; Mao, W.; Pan, W.; Guo, Y.; Xiong, Y.; Jin, H. Low-Temperature Thermoelectric Properties of β-Ag_2Se Synthesized by Hydrothermal Reaction. *J. Electron. Mater.* **2010**, *40*, 624–628. [CrossRef]
10. Xiao, C.; Xu, J.; Li, K.; Feng, J.; Yang, J.; Xie, Y. Superionic phase transition in silver chalcogenide nanocrystals realizing optimized thermoelectric performance. *J. Am. Chem. Soc.* **2012**, *134*, 4287–4393. [CrossRef]
11. Tsubota, T.; Ohtaki, M.; Eguchi, K.; Arai, H. Thermoelectric properties of Al-doped ZnO as a promising oxide material for high-temperature thermoelectric conversion. *J. Mater. Chem.* **1997**, *7*, 85–90. [CrossRef]
12. Wang, H.; Li, J.F.; Nan, C.W.; Zhou, M.; Liu, W.; Zhang, B.P.; Kit, T. High-performance $Ag_{0.8}Pb_{18+x}SbTe_{20}$ thermoelectric bulk materials fabricated by mechanical alloying and spark plasma sintering. *Appl. Phys. Lett.* **2006**, *88*, 092104. [CrossRef]
13. Venkatasubramanian, R.; Siivola, E.; Colpitts, T.; O'Quinn, B. Thin-film thermoelectric devices with high room-temperature figures of merit. *Nature* **2001**, *413*, 597–602. [CrossRef] [PubMed]
14. Choi, J.; Jeon, Y.; Cho, K.; Kim, S. Field-effect modulation of the thermoelectric characteristics of silicon nanowires on plastic substrates. *Nanotechnology* **2016**, *109*, 485401. [CrossRef]
15. Curtin, B.M.; Fang, E.W.; Bowers, J.E. Highly ordered vertical silicon nanowire array composite thin films for thermoelectric devices. *J. Electron. Mater.* **2012**, *41*, 887–894. [CrossRef]
16. Hochbum, A.I.; Chen, R.; Delgado, R.D.; Liang, W.; Garnett, E.C.; Najarian, M.; Majumdar, A.; Yang, P. Enhanced thermoelectric performance of rough silicon nanowires. *Nature* **2008**, *451*, 163–167. [CrossRef]
17. Boukai, A.I.; Bunimovich, Y.; Tahir-Kheli, J.; Yu, J.K.; Goddard III, W.A.; Heath, J.R. Silicon nanowires as efficient thermoelectric materials. *Nature* **2008**, *451*, 168–171. [CrossRef]
18. Zeng, X.; Yan, C.; Ren, L.; Zhang, T.; Zhou, F.; Liang, X.; Wang, N.; Sun, R.; Xu, J.B.; Wong, C.P. Silver Telluride Nanowire Assembly for High-Performance Flexible Thermoelectric Film and Its Application in Self-Powered Temperature Sensor. *Adv. Electron. Mater.* **2019**, *5*, 1800612. [CrossRef]

19. Zhou, C.; Dun, C.; Wang, K.; Zhang, X.; Shi, Z.; Liu, G.; Hewitt, C.A.; Qiao, G.; Carroll, D.L. General method of synthesis ultrathin ternary metal chalcogenide nanowires for potential thermoelectric applications. *Nano Energy* **2016**, *30*, 709–716. [CrossRef]
20. Xu, E.; Li, Z.; Acosta, J.A.; Li, N.; Swartzentruber, B.; Zheng, S.; Sinitsyn, N.; Htoon, H.; Wang, J.; Zhang, S. Enhanced thermoelectric properties of topological crystalline insulator PbSnTe nanowires grown by vapor. *Nano Res.* **2016**, *9*, 820–830. [CrossRef]
21. Choi, J.; Cho, K.; Yoon, D.S.; Kim, S. Thermal conductivity of silicon nanowires embedded on thermoelectric platforms. *Meas. Sci. Technol.* **2016**, *27*, 105007. [CrossRef]
22. Choi, J.; Cho, K.; Kim, S. Flexible thermoelectric generators composed of n-and p-type silicon nanowires fabricated by top-down method. *Adv. Energy Mater.* **2017**, *7*, 1602138. [CrossRef]
23. Yang, S.; Cho, K.; Park, Y.; Kim, S. Bendable thermoelectric generators composed of *p*-and *n*-type silver chalcogenide nanoparticle thin films. *Nano Energy* **2018**, *49*, 333–337. [CrossRef]
24. Seong, H.; Cho, K.; Kim, S. Photocurrent characteristics of solution-processed HgTe nanoparticle thin films under the illumination of 1.3 µm wavelength light. *Semicond. Sci. Technol.* **2008**, *23*, 075011. [CrossRef]
25. Jang, W.; Bao, W.; Jing, L.; Lau, C.N.; Dames, C. Thermal conductivity of suspended few-layer graphene by a modified T-bridge method. *Appl. Phys. Lett.* **2013**, *103*, 133102. [CrossRef]
26. Ghasemi, H.; Ni, G.; Marconnet, A.M.; Loomis, J.; Yerci, S.; Miljkovic, N.; Chen, G. Solar steam generation by heat localization. *Nat. Commun.* **2014**, *5*, 4449. [CrossRef]
27. Khuu, V.; Osterman, M.; Bar-Cohen, A.; Pecht, M. Considerations in the use of the laser flash method for thermal measurements of thermal interface materials. *IEEE Trans. Compon. Pack. Manuf. Technol.* **2011**, *1*, 1015–1028. [CrossRef]
28. Amirthan, G.; Udaya kumar, A.; Balasubramanian, M. Thermal conductivity studies on Si/SiC ceramic composites. *Ceram. Int.* **2011**, *37*, 423–426. [CrossRef]
29. Rolan, R.B.; Anaya, J.; Kuball, M. Thermal conductivity of bulk GaN–Effects of oxygen magnesium doping and strain field compensation. *Appl. Phys. Lett.* **2014**, *105*, 202105.
30. Sato, N.; Kuwabara, K.; Ono, K.; Sakata, T.; Morimura, H.; Terada, J.; Kudou, K.; Kamei, T.; Yano, M.; Machida, K.; et al. Monolithic integration fabrication process of thermoelectric and vibrational devices for microelectromechanical system power generator. *Jpn. J. Appl. Phys.* **2007**, *46*, 6062. [CrossRef]